Systematic Design of a Multiport MIMO Antenna With Bilateral Symmetry Based on Characteristic Mode Analysis

Dong-Woo Kim and Sangwook Nam, *Senior Member, IEEE*

***Abstract*— There are various bilaterally symmetric structures in the world. Characteristic mode analysis (CMA) enables to use a conductor with the symmetric structure itself as an antenna. Based on CMA, it is possible to implement a multiport MIMO antenna on the conductor using a mode-decoupling network (MDN). As the number of antennas increases, however, the complexity of the MDN becomes large, making design difficult. In this paper, we propose a simpler systematic design method for a multiport MIMO antenna on an electrically small and bilaterally symmetric conductor. More specifically, the implementation of the MDN depends on the design of the coupling elements that excite characteristic modes, so a design method for its position and shape is proposed. Owing to the well-designed coupling elements, a simple systematic design of the multiport MIMO antenna is suggested. The proposed design method is verified by simulation and measurement of a bug-like 3-port MIMO antenna operating in the 2.4 GHz ISM band, applicable to biomimetic drones. The antenna is realized using an FR-4 substrate with dimensions of 50 mm × 61.5 mm × 10 mm ($0.4\lambda_0 \times 0.49\lambda_0 \times 0.08\lambda_0$ at 2.4 GHz). The measurements demonstrate that these antennas have a low mutual coupling (<−20 dB) and a low envelope correlation coefficient (<0.04).**

***Index Terms*— Bilateral symmetry, characteristic current point correlation, characteristic mode analysis (CMA), MIMO antenna, mode-decoupling network (MDN), platform-mounted antenna.**

I. Introduction

MUCH effort is being devoted to increasing the data rate of today's communication systems. One way to increase capacity is by using multiple-in multiple-out (MIMO) communication [1], which can enhance capacity without broadening bandwidth. However, obtaining higher increases in channel capacity for an increase in the number of inputs or outputs requires some conditions to be met. In antenna design, uncorrelation and high isolation should be ensured between the antennas [1]. However, these features become more difficult to ensure as the distance between antennas diminishes.

Manuscript received January 4, 2017; revised November 13, 2017; accepted December 20, 2017. Date of publication December 27, 2017; date of current version March 1, 2018. This work is supported by a grant to Bio-Mimetic Robot Research Center funded by Defense Acquisition Program Administration, and by Agency for Defense Development (UD130070ID). *(Corresponding author: Sangwook Nam.)*

The authors are with the School of Electrical and Computer Engineering, Institute of New Media Communication, Seoul National University, Seoul 152742, South Korea (e-mail: cb3403@snu.ac.kr; snam@snu.ac.kr).

Color versions of one or more of the figures in this paper are available online at http://ieeexplore.ieee.org.

Digital Object Identifier 10.1109/TAP.2017.2787607

Characteristic mode analysis (CMA) is a suitable theory for an antenna design [2], [3]. It provides physical insights into the characteristics of an antenna, and therefore, can be applied to platform-mounted antenna designs [4]–[6]. This type of antenna can be designed intuitively by placing a coupling element for exciting a particular mode derived from CMA of the antenna platform. In addition, CMA also provides a set of basis currents that guarantee the orthogonality of the far-field patterns; therefore, it has been proposed for usage with various antennas for MIMO applications [7]–[14]. From the orthogonal property, matching each characteristic mode (CM) with an MIMO element antenna gives a low pattern correlation, which can be used for pattern diversity based MIMO antenna. Specifically, a 2-port MIMO antenna can be implemented through nothing more than proper design of coupling elements [7]–[10]. However, in the case of a multiport MIMO antenna design, individual excitation of each CM becomes difficult as more CMs are involved, because they are intertwined each other. For this reason, an additional mode-decoupling network (MDN) is required.

In fact, researches showed that the design of multiport MIMO antennas can be realized by constructing an MDN that is derived from eigenvalue decomposition of the *Z*-matrix or *S*-matrix of the antenna ports [15]–[17]. Like CMA, the antenna patterns created through the designed MDN also provide orthogonality. However, as the number of antennas grows, the complexity of the MDN increases considerably [17], and sometimes a certain amount of loss is required in the network [15]. In [16] and [17], it was suggested that the MDN can be easily implemented through symmetric design of the antennas and ports. On the other hand, studies combining the MDN and CMA were also conducted in [11] and [18]. In [18], it was shown that patterns of the MIMO antenna generated through the MDN derived from the *Z*-matrix coincide with the combination of the modal patterns, rather than each individual modal pattern. In [11], it was suggested that a simple MDN configuration is possible when the ports to excite CMs are designed symmetrically on a symmetric conductor. However, a multiport MIMO antenna design based on the method used in [11] requires a biaxially symmetric structure, as shown in Fig. 1(a).

In this paper, a simple method of designing a multiport MIMO antenna using CMA and MDN on an electrically small conductor with bilateral symmetry, as shown in Fig. 1(b),

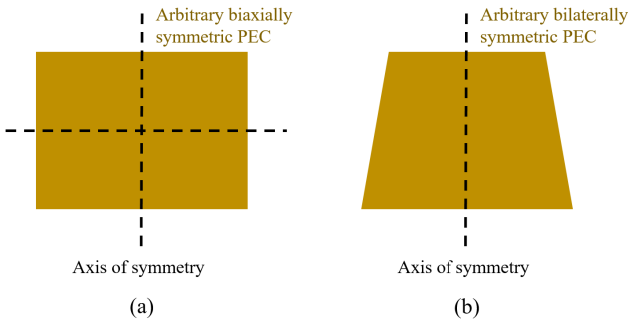

Fig. 1. Examples of (a) biaxially symmetric conductor and (b) bilaterally symmetric conductor.

is proposed, which is conceptually introduced in [19]. Since the design of the MDN and excitation of the CMs are determined by the coupling elements, a design method for these positions and shapes is suggested. In the case of a bilaterally symmetric conductor, CMs are classified into two groups, an even CM and an odd CM. Antennas using different CM groups (even and odd CMs) can be separated by designing coupling elements using structural symmetry. For a multiport extension, the separation between antennas using the same CM group (even or odd CMs) is required. However, since the mode currents in the same CM group are usually correlated, separating these antennas with only the coupling elements is difficult, so an additional MDN is required. However, owing to the separation of antennas using different CM groups, the MDN can be constructed more easily than the conventional MDN design method used in [15]. As a result, a systematic design of a 3-port MIMO antenna can be possible only with one conventional unequal 180° hybrid coupler for the MDN. For a 4-port MIMO antenna with two even CMs and two odd CMs, the design can be possible using two unequal 180° hybrid couplers.

This paper is organized as follows. In Section II, the theory of CMA is reviewed, the characteristic current point correlation is defined, the physical meaning of this correlation is found, and the coupling element is briefly reviewed. In Section III, the properties mentioned in Section II are applied to the positioning and shaping of the coupling elements. Also, a systematic design approach using MDN is developed for a multiport electrically small and bilaterally symmetric MIMO antenna. In Section IV, a 3-port MIMO antenna applicable to biomimetic drones is implemented in order to verify the proposed design method, which was proposed with simulation results in [20]. In Section V, conclusions about the finding are drawn.

II. Theory

A. Characteristic Mode Analysis (CMA)

The theory of the CM of conducting bodies was first introduced by Garbacz and Turpin [2] in 1968, and later refined by Harrington and Mautz [3] in 1971. It provides a basis set of current on the body, which has orthogonal properties of radiation. These basis currents are called characteristic currents, and they are determined by the following a generalized eigenproblem:

$$X\mathbf{J}_n = \lambda_n R\mathbf{J}_n \tag{1}$$

where λ_n is eigenvalue, $\mathbf{J}_n$ is characteristic current, and R and X are the real and imaginary parts of the MoM Z-matrix of the conductor. Since R and X are the real and symmetric matrices, all eigenvalues λ_n and characteristic currents $\mathbf{J}_n$ are real. Therefore, these CMs satisfy the orthogonal properties of radiation by the following three equations:

$$\begin{aligned}\langle \mathbf{J}_m, R\mathbf{J}_n\rangle &= \delta_{mn}\\ \langle \mathbf{J}_m, X\mathbf{J}_n\rangle &= \lambda_n\delta_{mn}\\ \langle \mathbf{J}_m, Z\mathbf{J}_n\rangle &= (1+j\lambda_n)\delta_{mn}\end{aligned} \tag{2}$$

where $\langle B, C\rangle = \iint B \cdot C ds$ and δ_{mn} is the Kronecker delta.

From CMA, the total current $\mathbf{J}$ on a conducting body can be expressed as a linear combination of the characteristic currents

$$\mathbf{J} = \sum_n \alpha_n \mathbf{J}_n \tag{3}$$

where α_n is the modal weighting coefficient (MWC) of the nth CM, and it can be calculated as

$$\alpha_n = \frac{\langle \mathbf{J}_n, \mathbf{E}^i_{\tan}\rangle}{1+j\lambda_n} \tag{4}$$

where $\mathbf{E}^i_{\tan}$ is the incident tangential E-field. The value of α_n determines how well the nth CM is excited. The numerator of the MWC is the modal excitation coefficient (MEC). This can be defined as (16) and is determined by how similarly a coupling element excites the nth CM. The denumerator of the MWC is related to the modal significance (MS) that satisfies (6), and it is determined by the resonant properties of the CM

$$\text{MEC} = \langle \mathbf{J}_n, \mathbf{E}^i\rangle \tag{5}$$

$$\text{MS} = \left|\frac{1}{1+j\lambda_n}\right|. \tag{6}$$

B. Characteristic Current Point Correlation

The characteristic current correlation is used to track the CM over frequency [21], or to find the MWC of the CM [22]. Like the characteristic current correlation, the characteristic current point correlation between the nth CM and the mth CM at the pth triangle mesh of the PEC can be defined as

$$\rho^{(p)}_{mn} = \frac{\langle \mathbf{J}^{(p)}_m, \mathbf{J}^{(p)}_n\rangle}{\|\mathbf{J}^{(p)}_m\|\,\|\mathbf{J}^{(p)}_n\|} \tag{7}$$

where the superscript (p) indicates the scalar or vector at the position of the pth triangle mesh. The characteristic current point correlation can be used as interpreting the MEC similarity of two CMs. As shown in Fig. 2, if the $\mathbf{J}^{(p)}_n$ is not orthogonal to the $\mathbf{J}^{(p)}_m$, then the $\mathbf{J}^{(p)}_n$ can be expressed as a linear combination of the $\mathbf{J}^{(p)}_m$ and its orthogonal vector $\mathbf{J}^{(p)\perp}_m$ as

$$\mathbf{J}^{(p)}_n = \frac{\langle \mathbf{J}^{(p)}_m, \mathbf{J}^{(p)}_n\rangle}{\|\mathbf{J}^{(p)}_m\|\,\|\mathbf{J}^{(p)}_m\|}\mathbf{J}^{(p)}_m + t\mathbf{J}^{(p)\perp}_m = \frac{\|\mathbf{J}^{(p)}_n\|}{\|\mathbf{J}^{(p)}_m\|}\rho^{(p)}_{mn}\mathbf{J}^{(p)}_m + t\mathbf{J}^{(p)\perp}_m \tag{8}$$

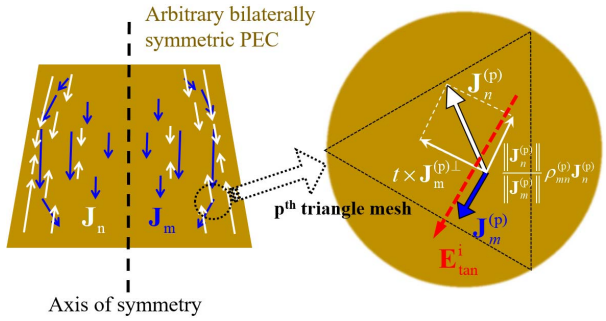

Fig. 2. Illustrative explanation of the vector notations of characteristic currents and assumed incident tangential E-field.

where t is an arbitrary constant. If the $\mathbf{E}^i_{\tan}$ has the same direction as the $\mathbf{J}^{(p)}_m$, as shown in Fig. 2, we can derive the MEC of the nth CM in terms of the $\mathbf{J}_m$ as

$$\langle \mathbf{J}_n, \mathbf{E}^i_{\tan} \rangle = \sum_{p=1}^{T} \left\langle \frac{\|\mathbf{J}^{(p)}_n\|}{\|\mathbf{J}^{(p)}_m\|} \rho^{(p)}_{mn} \mathbf{J}^{(p)}_m + t\mathbf{J}^{(p)\perp}_m, \mathbf{E}^{i(p)}_{\tan} \right\rangle = \sum_{p=1}^{T} \left\langle \frac{\|\mathbf{J}^{(p)}_n\|}{\|\mathbf{J}^{(p)}_m\|} \rho^{(p)}_{mn} \mathbf{J}^{(p)}_m, \mathbf{E}^{i(p)}_{\tan} \right\rangle \tag{9}$$

where T is the number of the triangle mesh. If the $\mathbf{E}^i_{\tan}$ by the coupling element is dominant around this coupling element and no significant change occurs in the characteristic currents around the coupling element, we can consider (14) as follows:

$$\langle \mathbf{J}_n, \mathbf{E}^i_{\tan} \rangle \approx \frac{\|\mathbf{J}^{(\mathrm{CE})}_n\|}{\|\mathbf{J}^{(\mathrm{CE})}_m\|} \rho^{(\mathrm{CE})}_{mn} \langle \mathbf{J}_m, \mathbf{E}^i_{\tan} \rangle \tag{10}$$

where the superscript CE means the scalar or vector near the coupling element, which can be assumed to have a constant value near the CE. Equation (15) implies that the MECs of the mth and nth CMs have a linear relationship in terms of the characteristic current point correlation. Thus, assuming that only two mth and nth dominant CMs exist and the coupling element is designed to fully excite the mth CM, the total current on the conductor consists of not only the mth CM, but also the nth CM as

$$\mathbf{J} = \sum_k \frac{\langle \mathbf{J}_k, \mathbf{E}^i_{\tan} \rangle}{1 + j\lambda_k} \mathbf{J}_k = \frac{\langle \mathbf{J}_m, \mathbf{E}^i_{\tan} \rangle}{1 + j\lambda_m} \mathbf{J}_m + \frac{\langle \mathbf{J}_n, \mathbf{E}^i_{\tan} \rangle}{1 + j\lambda_n} \mathbf{J}_n \approx \frac{\langle \mathbf{J}_m, \mathbf{E}^i_{\tan} \rangle}{1 + j\lambda_m} \mathbf{J}_m + \frac{\|\mathbf{J}^{(\mathrm{CE})}_n\|}{\|\mathbf{J}^{(\mathrm{CE})}_m\|} \rho^{(\mathrm{CE})}_{mn} \frac{\langle \mathbf{J}_m, \mathbf{E}^i_{\tan} \rangle}{1 + j\lambda_n} \mathbf{J}_n. \tag{11}$$

C. Coupling Element

An MIMO antenna using CMA has two design options for exciting a CM on the structure of the antenna: one employs inductive coupling elements (ICEs), and the other uses capacitive coupling elements (CCE) [23]. The CCE requires an additional component, whereas the ICE does not require any additional components because it can be simply obtained by making slots on the structure. For this reason, we utilize the ICE as the foundation of the design in this paper.

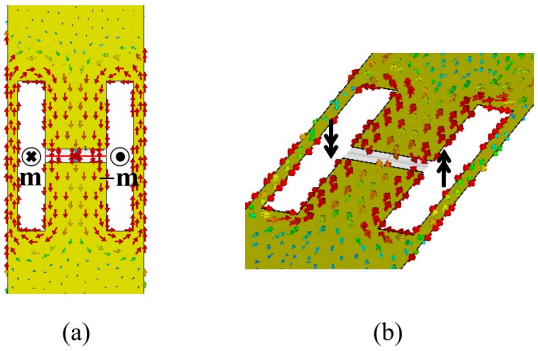

Fig. 3. Geometry of the H-shaped ICE [24]. (a) Top view. (b) 3-D view.

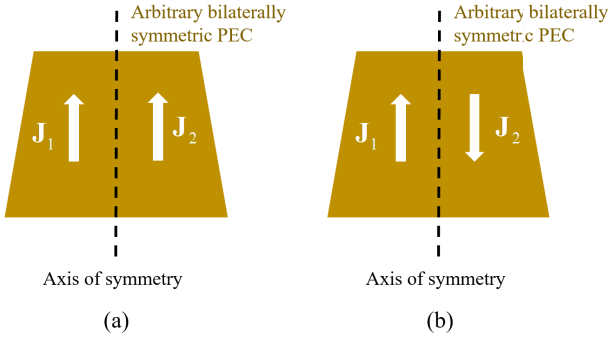

Fig. 4. Definition of (a) even CM and (b) odd CM for the bilaterally symmetric conductor.

As an example of the ICE, Won *et al.* [24] qualitatively suggests that the ICE design with an H-shaped slot can excite the desired CM more. As shown in Fig. 3, when the H-shaped ICE is excited, loop currents are formed on both sides, which can be modeled as the vertical magnetic dipole sources. Since these equivalent sources exist on both sides, desired CM is created more than the ICE presented in [23]. In this paper, this H-shaped ICE is applied to the antenna to be introduced in Section IV.

III. Proposed Design Method on an Electrically Small and Bilaterally Symmetric Structure

When CMA is applied to a bilaterally symmetric conductor, the CMs of the conductor can be divided into two groups with respect to the axis of symmetry, an even CM, and an odd CM [11]. As shown in Fig. 4, the total current flowing on the conductor can be divided into the currents flowing on the left side $\mathbf{J}_1$ and the currents flowing on the right side $\mathbf{J}_2$. The even CM is defined as a CM that has a current distribution of $\mathbf{J}_1 = \mathbf{J}_2$, and odd CM is defined as a CM that has a current distribution of $\mathbf{J}_1 = -\mathbf{J}_2$. The presence of even CM and odd CM on a bilaterally symmetric conductor is proven in the Appendix. In this section, a multiport MIMO antenna design method on an electrically small and bilaterally symmetric conductor based on the properties of even and odd CM is proposed.

A. Separation Among Antennas Using Different CM Groups (Even and Odd CMs)

Because of the symmetric nature of the even and odd CMs, separating between antennas using different CM groups is

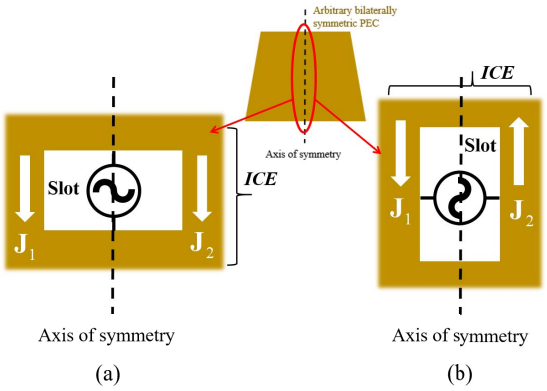

Fig. 5. Placement of the ICE. (a) ICE for exciting the even CMs. (b) ICE for exciting the odd CMs.

possible by properly designing the ICEs. The term "separation" refers to a condition that satisfies both individual excitation of the CM for each antenna and low coupling between the antennas. To separate these antennas, the ICEs are designed on the axis of symmetry, as shown in Fig. 5. For the antenna using the even CM, the ICE is should be on the line of the axis of symmetry, as shown in Fig. 5(a). For the antenna using the odd CM, the ICE should be perpendicular to the axis of symmetry, as shown in Fig. 5(b). Though it is unnecessary to design the slot as a rectangular shape, as shown in Fig. 5, the slot should be formed symmetrically with respect to the axis of symmetry. If the above condition is satisfied, the ICE as shown in Fig. 5(a) excites only the even CMs, and the ICE as shown in Fig. 5(b) excites only the odd CMs because of the properties of symmetry. In addition, due to their structural orthogonality, the ports between these two ICEs are virtually open, thus ensuring low coupling between ports.

B. Separation Among Antennas Using the Same CM Group (Even or Odd CMs)

If we separate among the antennas using different CM groups, a 2-port MIMO antenna design can be implemented easily. However, for an extension to a multiport MIMO antenna, the multiple even or odd CMs must be used individually for each antenna. Therefore, the antennas using the same CM group are necessary to be separated. However, the method used in Section III-A does not guarantee separation among these antennas, and the primary reason for this is that the characteristic current point correlation of the same CM group is mostly nonzero around the ICE. Therefore, the designed ICE cannot excite the desired CM individually. In addition, among these ICEs, a high rate of coupling exists because they excite not only the same dominant modes, but also same higher order modes, which increases coupling.

For these reason, the proposed solution is utilization of an MDN. By using the information of CMA, a simple MDN design can be created. The first step is to determine the position and shape of the ICE based on the information of CMA, especially the characteristic current point correlation. Knowing the characteristic current point correlation means knowing the ratio of the generated CMs by the ICE. It implies that the ICE can be designed to make the MDN easy to configure by matching the ratio. When there are only two CMs in the same CM group, the MDN design using unequal 180° hybrid coupler can be done as follows. First, the characteristic current point correlation at the entire conductor is calculated. Second, two positions for the ICEs are determined that matches the ratio of the CMs and the signal ratio of the hybrid coupler. Finally, two ICEs are designed iteratively at the obtained areas to more precisely meet the ratio that hybrid coupler is required. After design of the ICEs, the final step is to design the unequal 180° hybrid coupler for the MDN. The detailed explanation of relationship between the characteristic current point correlation and the unequal 180° hybrid coupler is as follows.

It is assumed that there are only two dominant CMs in the same CM group. To design two element MIMO antennas, two ICEs are required; ICE1 and ICE2. The currents produced or received by each ICE are called $\mathbf{J}_{\mathrm{ICE1}}$ and $\mathbf{J}_{\mathrm{ICE2}}$, and the incident E-fields produced by each ICE are called $\mathbf{E}^i_{\mathrm{ICE1}}$ and $\mathbf{E}^i_{\mathrm{ICE2}}$. Since ρ_{mn} is typically nonzero, $\mathbf{J}_{\mathrm{ICE1}}$ and $\mathbf{J}_{\mathrm{ICE2}}$ can be obtained using (11) as

$$\begin{aligned}\mathbf{J}_{\mathrm{ICE1}} &\approx \frac{\langle \mathbf{J}_m, \mathbf{E}^i_{\mathrm{ICE1}}\rangle}{1+j\lambda_m}\mathbf{J}_m + \frac{\langle \mathbf{J}_n, \mathbf{E}^i_{\mathrm{ICE1}}\rangle}{1+j\lambda_n}\mathbf{J}_n \\ &\approx \frac{\langle \mathbf{J}_m, \mathbf{E}^i_{\mathrm{ICE1}}\rangle}{1+j\lambda_m}\mathbf{J}_m + \frac{\|\mathbf{J}_n^{(\mathrm{ICE1})}\|}{\|\mathbf{J}_m^{(\mathrm{ICE1})}\|}\rho_{mn}^{(\mathrm{ICE1})}\frac{\langle \mathbf{J}_m, \mathbf{E}^i_{\mathrm{ICE1}}\rangle}{1+j\lambda_n}\mathbf{J}_n\end{aligned} \tag{12}$$

$$\begin{aligned}\mathbf{J}_{\mathrm{ICE2}} &\approx \frac{\langle \mathbf{J}_m, \mathbf{E}^i_{\mathrm{ICE2}}\rangle}{1+j\lambda_m}\mathbf{J}_m + \frac{\langle \mathbf{J}_n, \mathbf{E}^i_{\mathrm{ICE2}}\rangle}{1+j\lambda_n}\mathbf{J}_n \\ &\approx \frac{\|\mathbf{J}_m^{(\mathrm{ICE2})}\|}{\|\mathbf{J}_n^{(\mathrm{ICE2})}\|}\rho_{mn}^{(\mathrm{ICE2})}\frac{\langle \mathbf{J}_n, \mathbf{E}^i_{\mathrm{ICE2}}\rangle}{1+j\lambda_m}\mathbf{J}_m + \frac{\langle \mathbf{J}_n, \mathbf{E}^i_{\mathrm{ICE2}}\rangle}{1+j\lambda_n}\mathbf{J}_n\end{aligned} \tag{13}$$

where the superscript ICE refers to the vector or scalar near the ICE. As mentioned, the MDN is designed using the conventional unequal (or equal) 180° hybrid coupler, especially rat-race coupler (RRC). The RRC outputs the signals for $\mathbf{J}_m$ on the $\sum$-port and $\mathbf{J}_n$ on the Δ-port from the two input signals $\mathbf{J}_{\mathrm{In1}}$ and $\mathbf{J}_{\mathrm{In2}}$, respectively, as

$$\mathbf{J}_{\mathrm{In1}} = ck\mathbf{J}_m - c\sqrt{1-k^2}\mathbf{J}_n \tag{14}$$

$$\mathbf{J}_{\mathrm{In2}} = c\sqrt{1-k^2}\mathbf{J}_m + ck\mathbf{J}_n \tag{15}$$

where c is an arbitrary constant and k is the coupling coefficient of the RRC [25]. As shown in Fig. 6, if two ICEs exciting two combined CMs are connected to the RRC, the signal coming from each ICE to the inputs of the RRC are as (12) and (13). When these incoming signals of the RRC satisfy (14) and (15), the individual CMs are generated at the output terminals of the RRC. That is, if the ICE is designed to satisfy the conditions $\mathbf{J}_{\mathrm{ICE1}} = \mathbf{J}_{\mathrm{In1}}$ and $\mathbf{J}_{\mathrm{ICE2}} = \mathbf{J}_{\mathrm{In2}}$ (or $\mathbf{J}_{\mathrm{ICE1}} = \mathbf{J}_{\mathrm{In2}}$, and $\mathbf{J}_{\mathrm{ICE2}} = \mathbf{J}_{\mathrm{In1}}$), the two combined CMs from the ICE can be separated through the RRC. The results for the above two conditions are as follows:

$$\begin{aligned}&\frac{\|\mathbf{J}_n^{(\mathrm{ICE1})}\|}{\|\mathbf{J}_m^{(\mathrm{ICE1})}\|}\rho_{mn}^{(\mathrm{ICE1})}\left|\frac{1}{1+j\lambda_n}\right|^2 \\ &\qquad = -\frac{\|\mathbf{J}_m^{(\mathrm{ICE2})}\|}{\|\mathbf{J}_n^{(\mathrm{ICE2})}\|}\rho_{mn}^{(\mathrm{ICE2})}\left|\frac{1}{1+j\lambda_m}\right|^2\end{aligned} \tag{16}$$

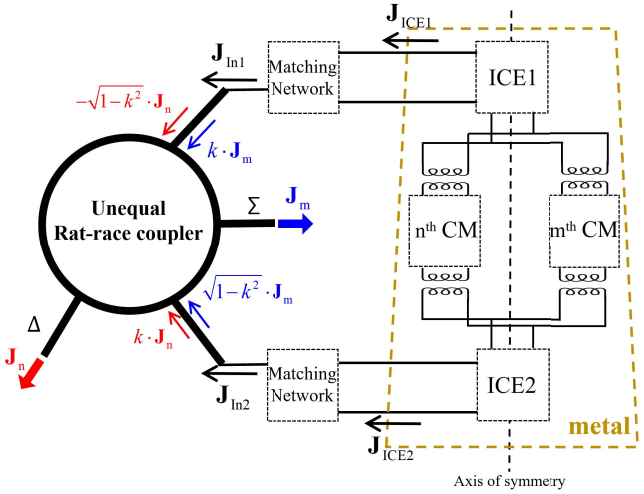

Fig. 6. Configuration of the MDN using RRC to separate the antenna using the same CM group.

$$\frac{\langle \mathbf{J}_m, \mathbf{E}^i_{\mathrm{ICE1}} \rangle}{1 + j\lambda_m} = \frac{\langle \mathbf{J}_n, \mathbf{E}^i_{\mathrm{ICE2}} \rangle}{1 + j\lambda_n} \tag{17}$$

$$k = \frac{\left| \frac{1}{1+j\lambda_m} \right|}{\sqrt{\left(\frac{1}{1+j\lambda_m} \right)^2 + \left(\frac{\left\| \mathbf{J}_n^{(\mathrm{ICE1})} \right\|}{\left\| \mathbf{J}_m^{(\mathrm{ICE1})} \right\|} \frac{\rho_{mn}^{(\mathrm{ICE1})}}{1+j\lambda_n} \right)^2}}. \tag{18}$$

Equation (16) depends only on the parameters of CMA. λ_m and λ_n are determined by the operating frequency. So, when the desired frequency is determined, the positions of ICE1 and ICE2 that satisfy (16) are found on the axis of symmetry. Equation (17) is related to MECs by each ICE, and it depends on the position and shape of the ICE. Since the position of the ICEs is derived from (16), the shape of the ICE is determined to satisfy (17) through the iterative EM simulation process. Finally, the coupling coefficient of the RRC is determined by (18). Equation (18) consists of the parameters of the CMA determined after the position of the ICE is selected by (16).

In conclusion, by designing an ICE and RRC that satisfy (16)–(18), individual CMs can be extracted at the output of the RRC. According to the reciprocity theorem, if the signal is applied to the $\sum$-port as a transmitting mode, it radiates through an antenna corresponding to mth CM. Similarly, if the signal is applied to the Δ-port, it radiates through an antenna corresponding to nth CM. In addition, the RRC guarantees isolation between two inputs or two outputs when all ports are connected to a 50 Ω system [25], which ensures high isolation between antennas using the same CM group.

C. Proposed Multiport MIMO Antenna System Configuration

Fig. 7 shows the system configuration for the proposed multiport MIMO antenna on an electrically small and bilaterally symmetric conductor. Fig. 7(a) is a system configuration of a 2-port MIMO antenna. Here, one antenna uses an even CM, and the other antenna uses an odd CM. As mentioned in Section III-A, the ICE design is sufficient for separating antennas using different CM groups. Fig. 7(b) shows the system configuration of a

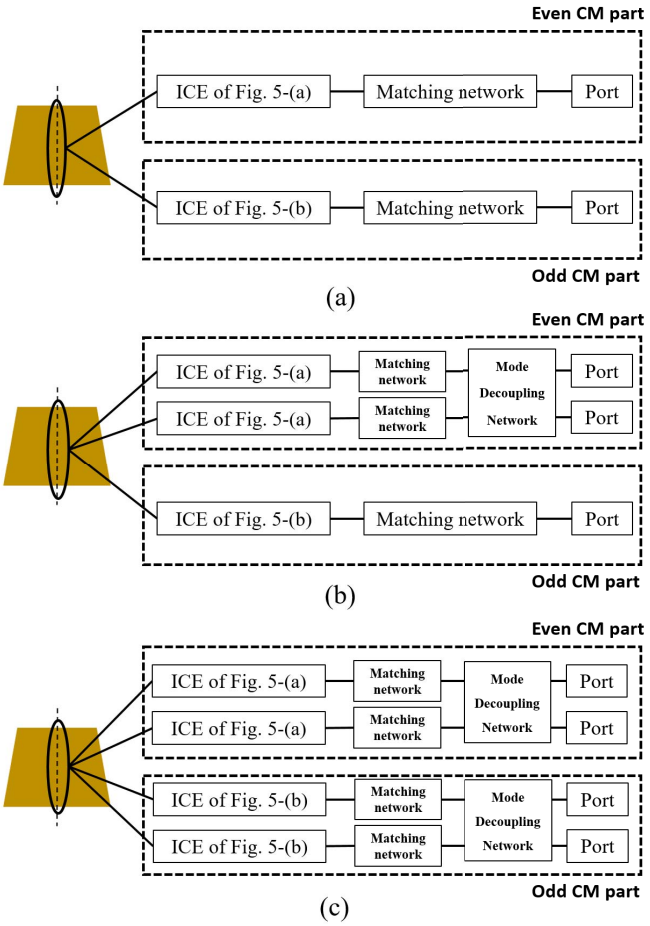

Fig. 7. Systematic configuration of the proposed MIMO antenna. (a) 2-port MIMO antenna system using one even CM and one odd CM. (b) 3-port MIMO antenna system using two even CMs and one odd CM. (c) 4-port MIMO antenna system using two even CMs and two odd CMs.

3-port MIMO antenna. Here, the two antennas use different even CMs individually, and the other antenna uses an odd CM. Similarly, the antenna using odd CMs is designed with the ICE alone. However, for the antennas using different even CMs, an additional MDN is required, as described in Section III-B. When the two antennas use different odd CMs individually and the other antenna uses an even CM, the system configuration is same as shown in Fig. 7(b), except designing an MDN at the odd CM part rather than the even CM part. While the existing method requires a 6-port MDN with three inputs and three outputs [15], the proposed systematic design requires only a 4-port MDN with two inputs and two outputs, which can reduce the design complexity of the MDN. Fig. 7(c) is a system configuration of a 4-port MIMO antenna and it can be only applied when two even CMs and two odd CMs are used as individual antennas. Even in this case, however, a much simpler implementation is possible, because two 4-port MDNs are required compared to the existing methods requiring an 8-port MDN [16].

IV. Example: Biomimetic Bug-Like MIMO Antenna

The proposed design method is verified by simulation and measurement of a bug-like 3-port MIMO antenna operating in

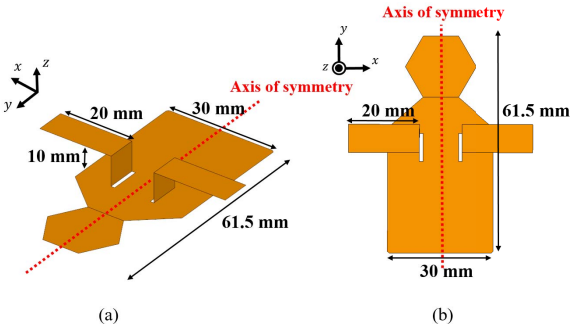

Fig. 8. Geometry of the biomimetic bug-like structure. (a) 3-D view. (b) Top view.

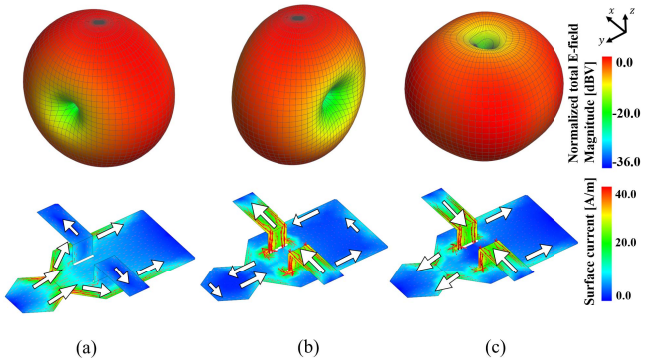

Fig. 9. Simulated normalized radiation patterns and surface current distribution of the first three dominant CMs of the platform at 2.4 GHz. (a) Mode 1. (b) Mode 2. (c) Mode 3.

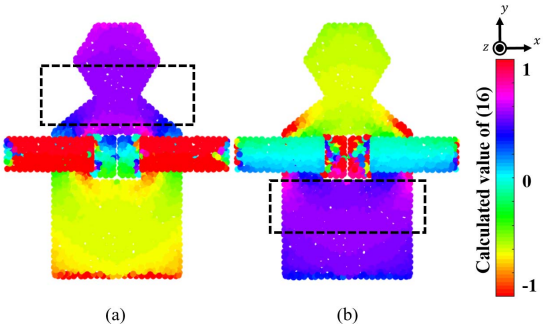

Fig. 10. Calculated results of (16) for every point of the structure with the ICE for odd CM. (a) Results for the left side of (16). (b) Results for the right side of (16). Since the values are mostly present between −1 and 1, values greater than 1 or less than −1 are treated as 1, −1 for better explanation.

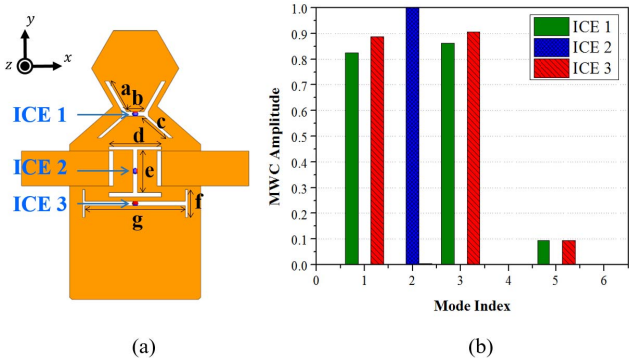

Fig. 11. (a) Geometry of a structure including H-shaped slots: $a = 8$ mm, $b = 4$ mm, $c = 7.5$ mm, $d = 12$ mm, $e = 9.8$ mm, $f = 6.4$ mm, and $g = 23$ mm. (b) Simulated MWC for each antenna port.

the 2.4 GHz ISM band, applicable to biomimetic drones. The biomimetic flapping-wing robot has been reported in many studies and can be used as a drone for military applications [26], [27]. These robots need antennas for communication; however, the arrangement of the antennas is burdensome compared to the size of the robots. For this reason, research has been conducted to use a robot frame as an antenna [20], [24]. In [24], a single-mode bug-like antenna design was developed based on the CMA with a similar platform as that of this paper. In [20], we present a simulated 3-port MIMO antenna on a bug-like platform, which is same as the model in this paper as shown in Fig. 8. In this paper, a more detailed design method of the 3-port MIMO antenna is described and the measurement results are shown. The program CST 2016 (Computer Simulation Technology) [28] and FEKO Suite 7.0 [29] were used for EM simulation and CMA.

A. CMA of a Bug-Like Structure

In the first design step, the CMA of the bug-like conducting body, as shown in Fig. 8, with dimensions of 50 mm × 61.5 mm × 10 mm ($0.4\lambda_0 \times 0.49\lambda_0 \times 0.08\lambda_0$ at 2.4 GHz), is performed to find the available set of modes at the 2.4 GHz ISM band. Fig. 9 shows the current distribution and radiation pattern for the first three dominant CMs with MS of 0.98, 0.92, and 0.38 at 2.4 GHz, respectively. Examination of the current distribution of each mode shows that modes 1 and 3 have even currents and mode 2 has odd current. Therefore, the system configuration of Fig. 7(b) is used.

B. ICE Design Based on the Proposed Method

In the next design step, to excite the first three CMs, respectively, the ICEs are designed on the conductor based on the design method proposed in Section III. First, the ICE should be placed on the axis of symmetry, the ICE for the even CM should be designed as Fig. 5(a), and the ICE for the odd CM should be designed as Fig. 5(b). The ICE for the odd CM is designed first; then the ICEs for the even CMs are designed. The ICE for odd CM is designed only to satisfy the condition of Fig. 5(b) with increasing the MEC for increasing the radiation resistance. In the case of ICEs for even CMs, they should be located at a position satisfying not only the condition of Fig. 5(a) but also (16). Fig. 10(a) shows the values of the left side of (16) at all points of the conductor and Fig. 10(b) shows the values of the right side of (16) at all points of the conductor. Based on this illustration, two proper regions to place the ICEs are derived as shown in the rectangular areas in Fig. 10. After determining the position of the ICE, the ICEs for the even CMs are designed to satisfy (17) iteratively, increasing the MEC.

In this paper, we use the H-shaped ICE mentioned in Section II-C to get the high MEC. Fig. 11(a) shows the result of designing the ICE so that the radiation resistance

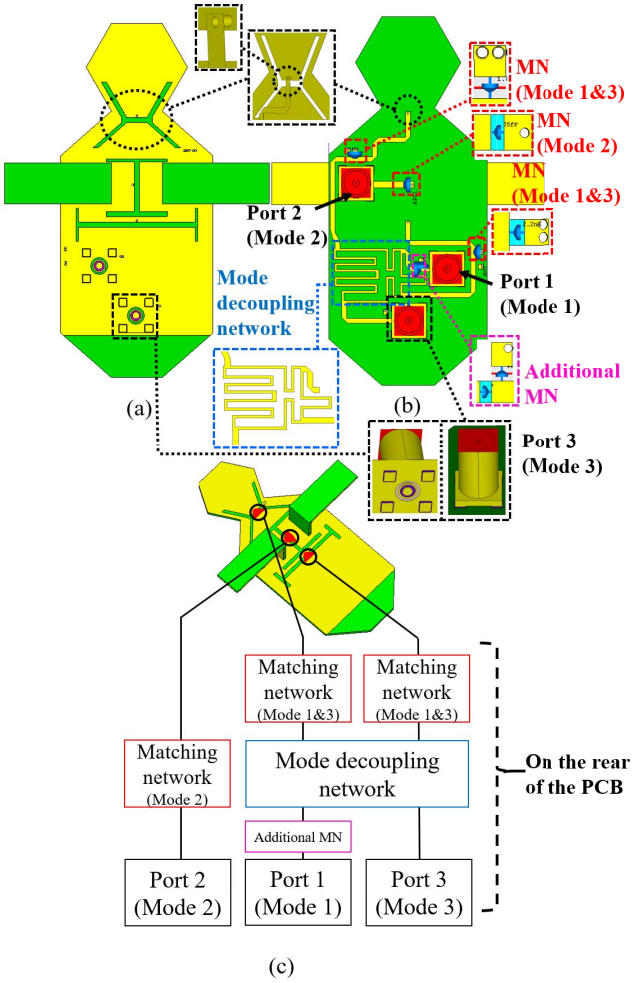

Fig. 12. Configuration of the proposed bug-like MIMO antenna including the feeding network. (a) Top view. (b) Bottom view. (c) Systematic view.

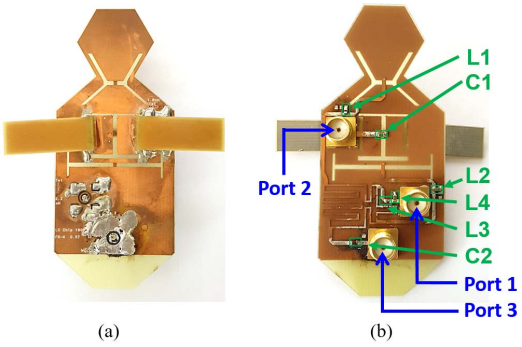

Fig. 13. Prototype of the manufactured antenna. (a) Top view. (b) Bottom view. C_2, C_1, and L_3 are in series and L_1, L_2, and L_4 are in shunt.

is close to 50 Ω. Fig. 11(b) shows the MWC of the ICE at 2.4 GHz, which shows that ICE1 and ICE3 excites both mode 1 and mode 3, and ICE2 excites only mode 2. The input impedance of each antenna port at 2.4 GHz is as follows: $Z_{\text{ICE1}} = 70.5 + j147.8$, $Z_{\text{ICE2}} = 34.9 + j142.5$, and $Z_{\text{ICE3}} = 76.7 + j164.1$.

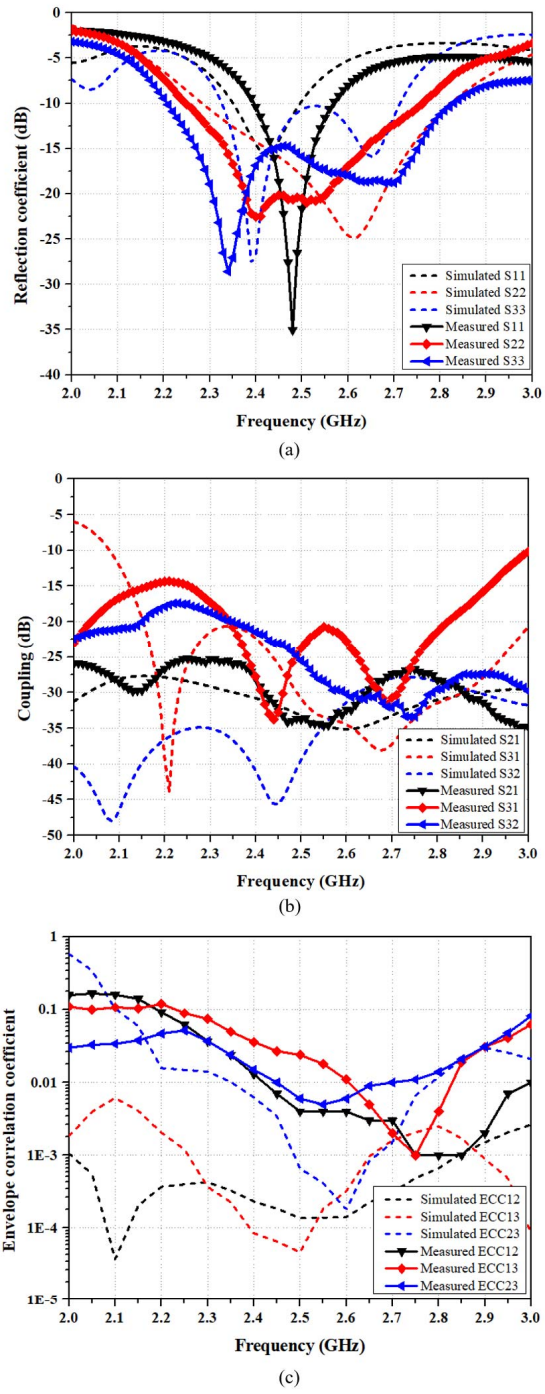

Fig. 14. Simulation and measured results of the proposed bug-like 3-port MIMO antenna. (a) Reflection coefficient. (b) Coupling. (c) ECC.

C. Systematic Design

The last design step involves the design of the matching network and feeding network, including the MDN. One advantage of CMA is that the structure of the antenna can be utilized as a ground for a transmission line. The transmission line can therefore be designed as a microstrip line, utilizing the structure of the antenna as a ground plane and designing the signal line of the microstrip line at the rear of the structure of the antenna, as shown in Fig. 12(a) and (b). A single-

TABLE I
COMPARISON OF THE IMPLEMENTED PERFORMANCES AND FEATURES FOR THE PROPOSED AND REFERENCE MULTIPORT MIMO ANTENNAS

	This work	[12]	[13]	[14]	[15]	[16]	[18]
Number of axis of symmetry	1	2	2	2	-	-	0
Number of element antenna	3	4	3	4	3	4	3
Additional configuration of feeding network	4-port MDN (1 coupler)	8-port MDN	5 power divider	1 coupler + 3 power divider	6-port MDN (2 couplers + air-bridge)	8-port MDN (4 couplers)	6-port MDN
Electrical size of the antenna w.r.t center freq.	$0.25\lambda_0 \times 0.51\lambda_0 \times 0.08\lambda_0$	$0.46\lambda_0 \times 0.46\lambda_0 \times 0.29\lambda_0$	$0.5\lambda_0 \times \lambda_0$	$\lambda_0 \times \lambda_0$	-	-	$0.8\lambda_0 \times 0.4\lambda_0$

layer FR-4 substrate($\varepsilon_r = 4.3$, $\tan\delta = 0.025$, and thickness is 0.5 mm) is used, and the conductor shown in Fig. 11(a) is placed at the top of the substrate, and matching networks MDN and feed network are designed on the rear side. The ICE is fed at the junction between the front and backsides, which is designed to be shorted to the microstrip line. The matching networks convert the input impedances Z_{ICE1}, Z_{ICE2}, and Z_{ICE3} into 50 Ω. The matching networks consist of series or shunt L and C. The MDN is designed with the conventional RRC with a coupling coefficient of $k = 1/\sqrt{2}$, which is designed by meandering the line for a compact design. In addition, we put a supplementary matching network after the RRC to compensate for some frequency shifting. An overview of the system is shown in Fig. 12(c).

D. Measurement and Results

The realized antenna shown in Fig. 13 is built following the simulated model dimensions. The commercially available capacitor and inductor are used for matching: $L_1 = 1.8$ nH, $C_1 = 75$ fF, $L_2 = 2.2$ nH, $C_2 = 1$ μF, $L_3 = 1.1$ nH, and $L_4 = 5.6$ nH. Fig. 14(a) and (b) shows the simulated and measured S-parameters of the proposed antenna. The measured −10 dB bandwidth is as follows: 2.4–2.56 GHz (Mode 1), 2.25–2.76 GHz (Mode 2), and 2.21–2.82 GHz (Mode 3). The coupling of both measured and simulation results is met under −20 dB, which is acceptable for MIMO applications. The envelope correlation coefficient is plotted against frequency in Fig. 14(c) and is calculated as

$$\rho_{m,n} = \frac{\left|\iint \mathbf{E}_m \cdot \mathbf{E}_n^* d\Omega\right|^2}{\iint |\mathbf{E}_m|^2 d\Omega \cdot \iint |\mathbf{E}_n|^2 d\Omega}. \tag{19}$$

The measured and simulated envelope correlation coefficient (ECC) are smaller than 0.1 in the 2.4 GHz ISM band, guaranteeing pattern diversity.

The radiation patterns of the proposed prototype are measured in an anechoic chamber. Fig. 15 shows the simulated and measured radiation patterns at 2.4 GHz. In addition, the modal patterns with normalized to simulated patterns are plotted together. The patterns for each port are measured when the other ports are matched with 50 Ω, and their measured efficiencies are 51.17%, 83.60%, and 52.87%, respectively. This shows that efficiency will not be a problem since most losses are due to the FR-4 substrate in the feeding network.

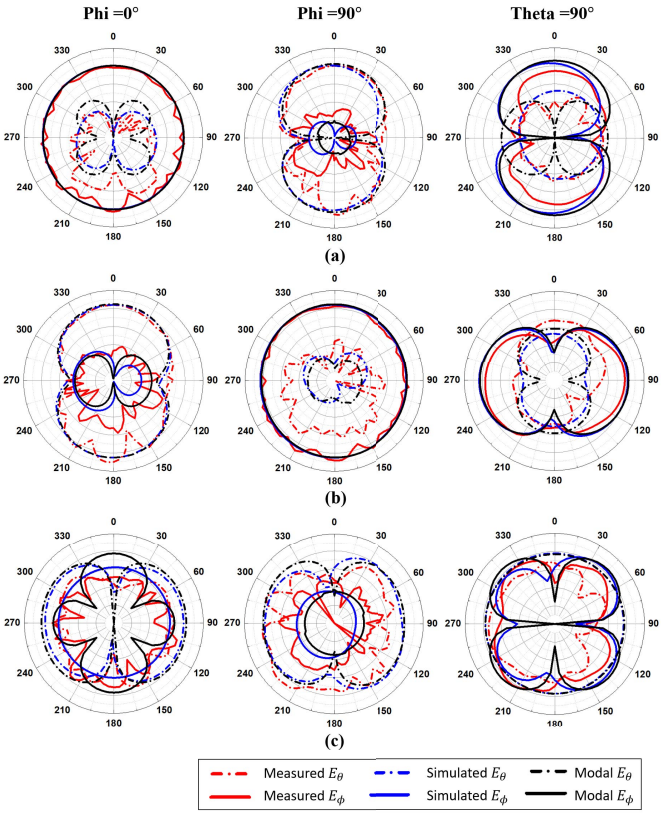

Fig. 15. Simulated and measured far-field 2-D patterns at 2.4 GHz. (a) Port 1 excitation. (b) Port 2 excitation. (c) Port 3 excitation.

Replacing the FR-4 with a less lossy substrate would improve performance considerably.

A comparison of the proposed antenna and the recently reported multiport MIMO antenna is presented in Table I. In [12]–[14] and [18], CMA-based design of multiport MIMO antennas were suggested. Two symmetric axes were used to implement a simple network in [12]–[14], and a 6-port MDN derived from characteristic port mode analysis was used without any symmetry in [18]. The design in [15] and [16] suggested MDN from the eigen-decomposition of N-port Z-matrix, but not based on CMA. By comparison, a simpler 3-port MIMO antenna system is proposed than the reference papers.

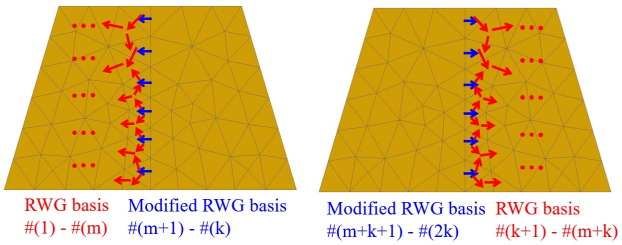

Fig. 16. Illustrative representation of the modified RWG basis. (a) RWG basis on the left side. (b) RWG basis on the right side.

V. Conclusion

In this paper, a simple multiport MIMO antenna design method on an electrically small and bilaterally symmetric conductor is proposed. The key design is provided by separating antennas using different CM groups with the properly designed ICEs. For this reason, only the separation among the antennas using the same CM group is needed. In addition, for an electrically small structure, the ICE can be designed to match the ratio of the CMs with the signal ratio of the RRC, which enables to design MDN with a conventional hybrid coupler. The conditions for matching the ratios are suggested mathematically, and these are the detailed guideline of the ICE design. In the case of a 3-port MIMO antenna using two even CMs and one odd CM (or two odd CMs and one even CM), it is possible to easily implement an MDN through only one RRC. In the case of a 4-port MIMO antenna using two even CMs and two odd CMs, it is possible to easily implement an MDN using two RRCs. As a result, the proposed design method can be applied to many electrically small and bilaterally symmetric platforms, such as cars, airplanes, and ships.

Appendix
Proof of Existence of the Even/Odd Characteristic Mode in Bilateral Symmetry

In the case of a bilaterally symmetric structure, the PEC can be decomposed into a Rao–Wilton–Glisson (RWG) basis. When making the RWG basis symmetric with respect to the axis of symmetry, we define #1 to #m of the RWG basis on the left side of the plane, #$(k+1)$ to #$(k+m)$ of RWG basis on the right side. To consider the basis on the axis of symmetry, the RWG basis on the axis of symmetry is modified. As shown in Fig. 16, the basis on the axis is split into the left and right halves. That is, the weighted sum of the currents by two bases determines the current perpendicular to the axis of symmetry. So, the modified RWG basis on the left side of axis is defined #$(m+1)$ to #(k) of RWG basis as shown in Fig. 16(a), and the modified RWG basis on the right side of axis is defined #$(k+m+1)$ to #$(2k)$ of RWG basis as shown in Fig. 16(b). From the defined RWG basis, a block Z-matrix of the structure can be derived based on the properties of symmetry as

$$Z_1 = Z(1:k, 1:k) = Z(k+1:2k, k+1:2k) \quad \text{(A1)}$$

$$Z_2 = Z(1:k, k+1:2k) = Z(k+1:2k, 1:k) \quad \text{(A2)}$$

where Z_1 consists of the RWG bases on the left side of the PEC and Z_2 consists of the RWG bases on the right side of the PEC. By (A1) and (A2), the total Z-matrix of the PEC with bilateral symmetry can be defined as follows:

$$Z = \begin{bmatrix} Z_1 & Z_2 \\ Z_2 & Z_1 \end{bmatrix} \quad \text{(A3)}$$

where $Z_1, Z_2 \in \mathbf{R}^{k\times k}$, $Z \in \mathbf{R}^{2k\times 2k}$. From (A3), we find that the Z-matrix of the PEC is a 2-by-2 block centrosymmetric matrix.

As mentioned above, the CMA solves the generalized eigenproblem of (1), and the same can be said for a bilaterally symmetric structure. The eigenvalue of the problem is obtained by finding λ_n, satisfying equation

$$\mathrm{Det}(X - \lambda_n R) = 0. \quad \text{(A4)}$$

The characteristic polynomial is also a 2×2 block centrosymmetric matrix, so one of the well-known properties of the 2-by-2 centrosymmetric matrix can be applied, and its determinant is calculated by the following equation:

$$\mathrm{Det}\begin{pmatrix} A & B \\ B & A \end{pmatrix} = \mathrm{Det}(A+B) * \mathrm{Det}(A-B). \quad \text{(A5)}$$

Now, (A4) yields

$$\begin{aligned} \mathrm{Det}(X - \lambda_n R) &= \mathrm{Det}\begin{pmatrix} X_1 - \lambda_n R_1 & X_2 - \lambda_n R_2 \\ X_2 - \lambda_n R_2 & X_1 - \lambda_n R_1 \end{pmatrix} \\ &= \mathrm{Det}(X_1 + X_2 - \lambda_n(R_1 + R_2)) \\ &\quad * \mathrm{Det}(X_1 - X_2 - \lambda_n(R_1 - R_2)) = 0 \end{aligned} \quad \text{(A6)}$$

where R_1 is the real part of Z_1, X_1 is the imaginary part of Z_1, and R_2 and X_2 are the real and imaginary parts of Z_2. From (A6), we derive the eigenvalue as

$$\lambda = \{\lambda_n | \mathrm{Det}(X_1 + X_2 - \lambda_n(R_1 + R_2) = 0\} \quad \text{(A7)}$$

or

$$\{\lambda_n | \mathrm{Det}(X_1 - X_2 - \lambda_n(R_1 - R_2) = 0\}. \quad \text{(A8)}$$

After calculating the eigenvalues, the characteristic current can be calculated using

$$\begin{bmatrix} X_1 & X_2 \\ X_2 & X_1 \end{bmatrix}\begin{bmatrix} \mathbf{J}_{n,1} \\ \mathbf{J}_{n,2} \end{bmatrix} = \lambda_n \begin{bmatrix} R_1 & R_2 \\ R_2 & R_1 \end{bmatrix}\begin{bmatrix} \mathbf{J}_{n,1} \\ \mathbf{J}_{n,2} \end{bmatrix} \quad \text{(A9)}$$

where $\mathbf{J}_{n,1}, \mathbf{J}_{n,2} \in \mathbf{R}^{k\times 1}$ and $\mathbf{J}_{n,1}$ mean the nth characteristic current that flows on the #1 to #k of RWG basis and $\mathbf{J}_{n,2}$ is the current that flows on the other RWG basis. The solution of (A9) will be derived by adding and subtracting the simultaneous equations, so it becomes

$$[X_1 + X_2 - \lambda_n(R_1 + R_2)](\mathbf{J}_{n,1} + \mathbf{J}_{n,2}) = 0 \quad \text{(A10)}$$

and

$$[X_1 - X_2 - \lambda_n(R_1 - R_2)](\mathbf{J}_{n,1} - \mathbf{J}_{n,2}) = 0. \quad \text{(A11)}$$

In (A10), the equation is met when $\mathbf{J}_{n,1} = -\mathbf{J}_{n,2}$ for eigenvalues that satisfy (A8), which corresponds to the odd mode with respect to the axis of symmetry. For the eigenvalue of (A7), $\mathbf{J}_{n,1} = \mathbf{J}_{n,2}$ is obtained for the solution of (A11), which corresponds to the even mode. As a further explanation, in the

case of even CM, there is no current flowing perpendicular to the axis because the two bases on the axis are opposite direction with the same magnitude. On the other hand, the current for the odd CM flows perpendicular to the axis. Thus, we prove that two types of characteristic current exist in the case of a bilaterally symmetric structure, which correspond to the odd and even current.

REFERENCES

[1] L. Zheng and D. N. C. Tse, "Diversity and multiplexing: A fundamental tradeoff in multiple-antenna channels," *IEEE Trans. Inf. Theory*, vol. 49, no. 5, pp. 1073–1096, May 2003.

[2] R. J. Garbacz and R. Turpin, "A generalized expansion for radiated and scattered fields," *IEEE Trans. Antennas Propag.*, vol. 19, no. 3, pp. 348–358, May 1971.

[3] R. F. Harrington and J. R. Mautz, "Theory of characteristic modes for conducting bodies," *IEEE Trans. Antennas Propag.*, vol. AP-19, no. 5, pp. 622–628, Sep. 1971.

[4] Y. Chen and C.-F. Wang, "Electrically small UAV antenna design using characteristic modes," *IEEE Trans. Antennas Propag.*, vol. 62, no. 2, pp. 535–545, Feb. 2014.

[5] Y. Chen and C. F. Wang, "HF band shipboard antenna design using characteristic modes," *IEEE Trans. Antennas Propag.*, vol. 63, no. 3, pp. 1004–1013, Mar. 2015.

[6] T.-Y. Shih and N. Behdad, "Bandwidth enhancement of platform-mounted HF antennas using the characteristic mode theory," *IEEE Trans. Antennas Propag.*, vol. 64, no. 7, pp. 2648–2659, Jul. 2016.

[7] K. Kumar Kishor and S. V. Hum, "A pattern reconfigurable chassis-mode MIMO antenna," *IEEE Trans. Antennas Propag.*, vol. 62, no. 6, pp. 3290–3298, Jun. 2014.

[8] H. Li, Z. T. Miers, and B. K. Lau, "Design of orthogonal MIMO handset antennas based on characteristic mode manipulation at frequency bands below 1 GHz," *IEEE Trans. Antennas Propag.*, vol. 62, no. 5, pp. 2756–2766, May 2014.

[9] I. Szini, A. Tatomirescu, and G. F. Pedersen, "On small terminal MIMO antennas, harmonizing characteristic modes with ground plane geometry," *IEEE Trans. Antennas Propag.*, vol. 63, no. 4, pp. 1487–1497, Apr. 2015.

[10] C. Deng, Z. Feng, and S. V. Hum, "MIMO mobile handset antenna merging characteristic modes for increased bandwidth," *IEEE Trans. Antennas Propag.*, vol. 64, no. 7, pp. 2660–2667, Jul. 2016.

[11] B. Yang and J. J. Adamas, "Systematic shape optimization of symmetric MIMO antennas using characteristic modes," *IEEE Trans. Antennas Propag.*, vol. 64, no. 7, pp. 2668–2678, Jul. 2016.

[12] M. Bouezzeddine and W. L. Schroeder, "Design of a wideband, tunable four-port MIMO antenna system with high isolation based on the theory of characteristic modes," *IEEE Trans. Antennas Propag.*, vol. 64, no. 7, pp. 2679–2688, Jul. 2016.

[13] R. Martens and D. Manteuffel, "Systematic design method of a mobile multiple antenna system using the theory of characteristic modes," *IET Microw., Antennas Propag.*, vol. 8, no. 12, pp. 887–893, Sep. 2014.

[14] D. Manteuffel and R. Martens, "Compact multimode multielement antenna for indoor UWB massive MIMO," *IEEE Trans. Antennas Propag.*, vol. 64, no. 7, pp. 2689–2697, Jul. 2016.

[15] C. Volmer, J. Weber, R. Stephan, K. Blau, and M. A. Hein, "An eigen-analysis of compact antenna arrays and its application to port decoupling," *IEEE Trans. Antennas Propag.*, vol. 56, no. 2, pp. 360–370, Feb. 2008.

[16] J. C. Coetzee and Y. Yu, "Port decoupling for small arrays by means of an eigenmode feed network," *IEEE Trans. Antennas Propag.*, vol. 56, no. 6, pp. 1587–1593, Jun. 2008.

[17] A. Krewski and W. L. Schroeder, "N-port DL-MIMO antenna system realization using systematically designed mode matching and mode decomposition network," in *Proc. 42nd Eur. Microw. Conf.*, Amsterdam, The Netherlands, Oct./Nov. 2012, pp. 156–159.

[18] J. Ethier and D. A. McNamara, "An interpretation of mode-decoupled MIMO antennas in terms of characteristic port modes," *IEEE Trans. Magn.*, vol. 45, no. 3, pp. 1128–1131, Mar. 2009.

[19] D. W. Kim and S. Nam, "Design of chassis MIMO antenna using characteristic mode theory," in *Proc. Int. Symp. Antennas Propag. (ISAP)*, Phuket, Thailand, Oct./Nov. 2017.

[20] D.-W. Kim and S. Nam, "Systematic design of 3-port bug-like MIMO antenna based on theory of characteristic mode," in *Proc. 11th Eur. Conf. Antennas Propag. (EUCAP)*, Paris, France, Mar. 2017, pp. 2224–2227.

[21] M. Capek, P. Hazdra, P. Hamouz, and J. Eichler, "A method for tracking characteristic numbers and vectors," *Prog. Electromagn. Res. B*, vol. 33, pp. 115–134, 2011.

[22] J. Won, S. Jeon, and S. Nam, "Identifying the appropriate position on the ground plane for MIMO antennas using characteristic mode analysis," *J. Eletromagn. Eng. Sci.*, vol. 16, no. 2, pp. 119–125, Apr. 2016.

[23] R. Martens, E. Safin, and D. Manteuffel, "Inductive and capacitive excitation of the characteristic modes of small terminals," in *Proc. Loughborough Antennas Propag. Conf.*, Loughborough, U.K., Nov. 2011, pp. 1–4.

[24] J. Won, S. Yoon, and S. Nam, "Design of antenna for bug robot using characteristic mode," in *Proc. USNC-URSI Radio Sci. Meeting (Joint AP-S Symp.)*, Vancouver, BC, Canada, Jul. 2015, p. 179.

[25] D. M. Pozar, *Microwave Engineering*, 4th ed. Hoboken, NJ, USA: Wiley, 2005.

[26] R. J. Wood, "The first takeoff of a biologically inspired at-scale robotic insect," *IEEE Trans. Robot.*, vol. 24, no. 2, pp. 341–347, Apr. 2008.

[27] Y. Zou, W. Zhang, and Z. Zhang, "Liftoff of an electromagnetically driven insect-inspired flapping-wing robot," *IEEE Trans. Robot.*, vol. 32, no. 5, pp. 1285–1289, Oct. 2016.

[28] CST Corporation. (2016). *CST Microwave Studio (MWS)*. [Online]. Available: http://www.cst.com

[29] Altair Engineering, Inc. *FEKO Suite 7.0*. Accessed: 2016. [Online]. Available: http://www.feko.info

Dong-Woo Kim received the B.S. degree in electrical and electronics engineering from Chung-Ang University, Seoul, South Korea, in 2014, and the M.S. degree from Seoul National University, Seoul, in 2017, where he is currently pursuing the Ph.D. degree.

His current research interests include characteristic mode analysis and electromagnetic analysis.

Sangwook Nam (S'87–M'88–SM'11) received the B.S. degree in electrical engineering from Seoul National University, Seoul, South Korea, in 1981, the M.S. degree in electrical engineering from the Korea Advanced Institute of Science and Technology, Seoul, in 1983, and the Ph.D. degree in electrical engineering from The University of Texas at Austin, Austin, TX, USA, in 1989.

From 1983 to 1986, he was a Researcher with the Gold Star Central Research Laboratory, Seoul. Since 1990, he has been a Professor with the School of Electrical Engineering and Computer Science, Seoul National University. His current research interests include analysis/design of electromagnetic structures, antennas, and microwave active/passive circuits.